Chapter 3

A mathematical model of a two-layered flow in a catheterized oesophagus under the influence of peristaltic waves of dilating amplitude

3.1 Introduction

3.1.1 The physical model

The oesophagus is a long, muscular, tube-like structure inside the human body that swallows masticated food and finally pushes it into the stomach for digestion. However, its dysfunctions due to swallowing disorders, gastroesophageal reflux disease, peptic ulcer disease, gastroparesis, stomach cancer, Barrett's Oesophagus, oesophageal cancer, achalasia, etc. In oesophageal motility disorders, the oesophagus contracts but fails to push food bolus into the stomach, or it may not contract or relax. Further, contractions may be irregular. The upper oesophageal sphincter, the body of the oesophagus, or the cardiac sphincter may be a source of oesophageal

dysfunction. In achalasia, food is stuck above the sphincter. There are certain ways to overcome those disorders. Oesophageal manometry is one in which a thin, flexible catheter, also known as a nasogastric tube, is used to assess the strength and coordination of oesophageal muscle functions.

3.1.2 The literature

To summarise, in brief, the analytical work carried out to this end, we would like to cite Kanai et al. (1970) who theoretically formulated the changes in blood pressure when a catheter is inserted in an artery. Apart from many related results, they found that blood pressure increases immensely at the distal end when a catheter is inserted. His experimental validations, however, were not in good agreement, for which he attributed various reasons. Roos and Lykoudis (1971) analyzed the problem of peristaltic pumping of ureteral flow with the inserted catheter. They did not find the pressure distribution to change appreciably but showed that between the catheter and the urethral wall, there is a thin lubrication-type layer capable of sustaining high pressures. Back et al. (1992) indicated significant flow blockage effects with a catheter. They had used Wilson et al. (1988) for pressure difference. Back (1994) theoretically and experimentally evaluated time mean flow for a coronary artery with a catheter. The impacts on flow rate in a stenosed artery with an inserted catheter were investigated before and after angioplasty by Back et al. (1996). The flow rate was found to be inversely proportional to the catheter thickness. Srivastava and Rastogi (2010) observed a significant rise in impedance and wall shear stress if the catheter size increases even slightly. Many of the researchers such as El Misiery et al. (2002a), Srivastava (2007), Hayat et al. (2006), Hayat et al. (2008), Mekheimer and Kot (2008b) etc., investigated the flow behavior of chyme in gastrointestinal tract with endoscopy. Those researchers considered a catheterized single-layered fluid. Ledesma et al. (2013) considered the problem of blood flow in a catheterized artery in the presence of atherosclerosis. Medhavi and Singh (2012) investigated the effect of catheterization in a two-layered flow of Newtonian fluids with different viscosities. While considering the two-layered flow, they did not consider the mass conservation of the two layers separately. As a consequence, the results are qualitatively wrong, for instance, they deduced the shape of an interface which is independent of the viscosities, which is not acceptable. Another attempt on the

flow of a non-Newtonian nano-fluid through a two-layered concentric cylinder has been made with a complex wave propagation Zeeshan et al. (2022). However, that discusses different aspects of blood flow, not through the oesophagus. Brasseur et al. (1987) had pointed out such inaccuracies, presented a corrected model by applying mass conservation independently in the core and the peripheral layers, and obtained the correct interface. This was followed by several researchers who either modified wrong results of earlier authors or brought research to an advanced level (Rao and Usha (1995), Misra and Pandey (1999), Misra and Pandey (2001), Misra and Pandey (2002), Elshehawey and Gharsseldien (2004), Pandey et al. (2011)). In view of this, the model of Medhavi and Singh (2012) requires correction. We attempt to correct the model of Medhavi and Singh (2012) and present modified results for two-layered flows with catheterization. We intend to investigate particularly swallowing in oesophagus with Newtonian layers. Unlike them, we further consider progressively dilating wave amplitude so that the pressure in the distal part is higher, which was clinically reported (Kahrilas et al. (1995), Pandey et al. (2017)). We intend to get appropriate answers to particularly the following queries:

(i) What happens to the pressure distribution when a catheter is inserted into a patient's oesophagus?

(ii) What is the optimal length of the catheter inside the oesophagus while nasal feeding is required for a patient?

(iii) Whether nasal feeding continues or not, is it safe to feed the patient water or any liquid through the mouth when the catheter is inside the oesophagus?
And, of course, some more related information will be investigated.

3.2 Mathematical formulation of the problem

Out of the two layers, the outer one is called the peripheral layer, and the inner one is called the core. We consider a cylindrical tube of uniform cross-section that propagates peristaltic waves of dilating amplitude. Such peristaltic waves create higher pressure in the distal oesophagus, which is an experimentally verified fact

(Kahrilas et al. (1995)). The peristaltic wave with dilating amplitude is given by (Pandey et al. (2017))

$$H(Z,t) = a - be^{kZ}\cos^2\frac{\pi}{\lambda}(Z-ct), \tag{3.1}$$

where H, Z, t, a, b, k, λ and c represent respectively the wall displacement, the axial coordinate, time, the tube-radius, the amplitude of the wave, the amplitude dilation parameter, the wavelength, and the wave velocity. This consideration has modified and produced several new results related to oesophageal swallowing (Pandey et al. (2017), Pandey and Singh (2019), Pandey and Chandra (2020), Pandey et al. (2022), Pandey and Tiwari (2020)).

We further consider μ_p and μ_c as the viscosities, respectively, of the Newtonian fluids in the peripheral and the core layers. Let us then consider a thin tube called a catheter of radius a_c introduced co-axially in the cylindrical tube. We plan to derive solutions in the dimensionless form and the wave frame of reference, which reduces the governing equations to steady flow. The transformations are as follows: the wave frame parameters are on the left side, while the laboratory frame parameters are on the right side of the equality signs (Shapiro et al. (1969)):

$z = Z - t$; $r = R$; $u = U - 1$; $v = V$; $p = p$; $\psi = \Psi - r$; $q = \overline{Q} - 1 = q_c + q_p$; $q_c = \overline{Q}_c - T$, where $T = \displaystyle\int_0^1 H_1(z)dz$.

The governing equations are free from θ terms when considering axisymmetric flows. Therefore, Navier Stokes equations together with the continuity equation for axisymmetric flow through the above-considered geometry where the core layer interacts with the peripheral layer are given by, in cylindrical polar coordinates, as follows (Brasseur et al. (1987)):

$$\rho_p\Big(\frac{\partial u_p}{\partial t} + u_p\frac{\partial u_p}{\partial z} + v_p\frac{\partial u_p}{\partial r}\Big) = -\frac{\partial p}{\partial z} + \mu_p\nabla^2 u_p, \quad H_1 \le r \le H, \tag{3.2}$$

$$\rho_p\Big(\frac{\partial v_p}{\partial t} + u_p\frac{\partial v_p}{\partial z} + v_p\frac{\partial v_p}{\partial r}\Big) = -\frac{\partial p}{\partial r} + \mu_p(\nabla^2 - \frac{1}{r^2})v_p, \quad H_1 \le r \le H, \tag{3.3}$$

$$\frac{1}{r}\frac{\partial}{\partial r}(rv_p) + \frac{\partial}{\partial z}(u_p) = 0. \tag{3.4}$$

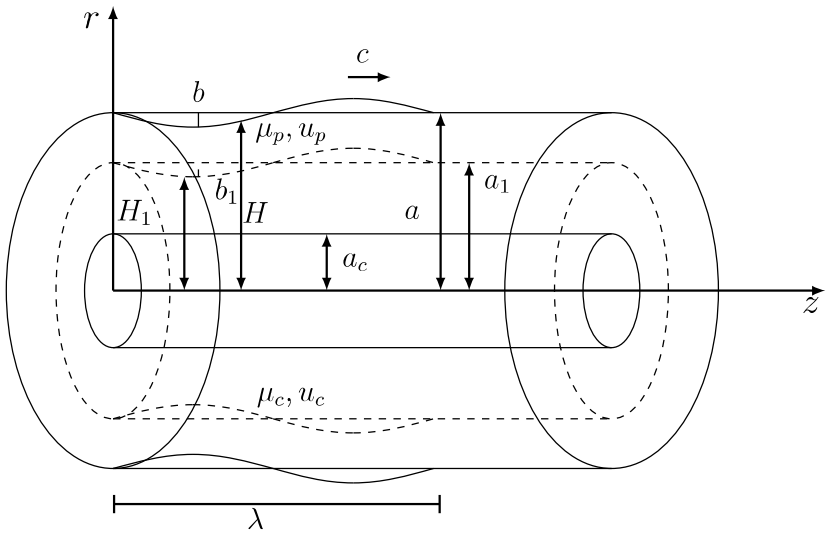

Figure 3.1: Geometry of a catheterised tube.

For the core layer,

$$\rho_c\Big(\frac{\partial u_c}{\partial t} + u_c\frac{\partial u_c}{\partial z} + v_c\frac{\partial u_c}{\partial r}\Big) = -\frac{\partial p}{\partial z} + \mu_c\nabla^2 u_c, \quad a_c \le r \le H_1, \tag{3.5}$$

$$\rho_c\Big(\frac{\partial v_c}{\partial t} + u_c\frac{\partial v_c}{\partial z} + v_c\frac{\partial v_c}{\partial r}\Big) = -\frac{\partial p}{\partial r} + \mu_c(\nabla^2 - \frac{1}{r^2})v_c, \quad a_c \le r \le H_1, \tag{3.6}$$

$$\frac{1}{r}\frac{\partial}{\partial r}(rv_c) + \frac{\partial}{\partial z}(u_c) = 0. \tag{3.7}$$

$\nabla^2 \equiv \frac{\partial^2}{\partial r^2} + \frac{1}{r}\frac{\partial}{\partial r} + \frac{\partial^2}{\partial z^2}$ is the Laplacian operator, r is the radial coordinate and p is the pressure. In the peripheral region u_p, v_p are the components of velocity and ρ_p is the fluid density, respectively, whereas in the core region u_c, v_c are the components of velocity and ρ_c is the fluid density.

According to the Misra and Pandey (2002), one may now assume $H_1 = a_1 - b_1 e^{kZ}\cos^2\frac{\pi}{\lambda}(Z-ct)$, where the amplitude for this interface wave is b_1. Non-dimensional variables are as follows
$(u_p', u_c') = \frac{(u_p,u_c)}{c}$, $r' = \frac{r}{a}$, $k' = k\lambda$, $b' = \frac{b}{a}$, $z' = \frac{z}{\lambda}$, $t' = \frac{ct}{\lambda}$, $(v_p', v_c') = \lambda\frac{(v_p,v_c)}{ac}$, $p' = \frac{a^2 p}{\lambda c\mu_c}$, $\mu = \frac{\mu_p}{\mu_c}$, using these variables from equations (3.2) to (3.7), we get

for the peripheral layer ($h_1 \leq r \leq h$)

$$\delta Re\Big(\frac{\partial u_p}{\partial t} + u_p\frac{\partial u_p}{\partial z} + v_p\frac{\partial u_p}{\partial r}\Big) = -\frac{\partial p}{\partial z} + \mu\Big(\frac{1}{r}\frac{\partial}{\partial r}(r\frac{\partial u_p}{\partial r}) + \delta^2\frac{\partial^2 u_p}{\partial z^2}\Big), \tag{3.8}$$

$$\delta^3 Re\Big(\frac{\partial v_p}{\partial t} + u_p\frac{\partial v_p}{\partial z} + v_p\frac{\partial v_p}{\partial r}\Big) = -\frac{\partial p}{\partial r} + \mu\Big(\delta^2\frac{1}{r}\frac{\partial}{\partial r}(r\frac{\partial v_p}{\partial r}) + \delta^4\frac{\partial^2 v_p}{\partial z^2} - \delta^2\frac{v_p}{r^2}\Big), \tag{3.9}$$

$$\frac{1}{r}\frac{\partial}{\partial r}(rv_p) + \frac{\partial u_p}{\partial z} = 0, \tag{3.10}$$

and for the core layer ($\epsilon \leq r \leq h_1$)

$$\Big(\frac{\rho_c}{\rho_p}\Big)Re\delta\Big(\frac{\partial u_c}{\partial t} + u_c\frac{\partial u_c}{\partial z} + v_c\frac{\partial u_c}{\partial r}\Big) = -\frac{\partial p}{\partial z} + \mu\Big(\frac{1}{r}\frac{\partial}{\partial r}(r\frac{\partial u_c}{\partial r}) + \delta^2\frac{\partial^2 u_c}{\partial z^2}\Big), \tag{3.11}$$

$$\Big(\frac{\rho_c}{\rho_p}\Big)Re\delta^3\Big(\frac{\partial v_c}{\partial t} + u_c\frac{\partial v_c}{\partial z} + v_c\frac{\partial v_c}{\partial r}\Big) = -\frac{\partial p}{\partial r} + \mu\Big(\delta^2\frac{1}{r}\frac{\partial}{\partial r}(r\frac{\partial v_c}{\partial r}) + \delta^4\frac{\partial^2 v_c}{\partial z^2} - \delta^2\frac{v_c}{r^2}\Big), \tag{3.12}$$

$$\frac{1}{r}\frac{\partial}{\partial r}(rv_c) + \frac{\partial u_c}{\partial z} = 0, \tag{3.13}$$

where
$h = \frac{H}{a} = 1 - \phi e^{k(z+t)}\cos^2(\pi z)$;
$h_1 = \frac{H_1}{a} = \alpha - \phi_1 e^{k(z+t)}\cos^2(\pi z)$; $\epsilon = \frac{a_c}{a}$; $(\alpha, \phi, \phi_1) = (a_1, b, b_1)/a$; $Re = \frac{\rho_p ac}{\mu_c}$; $\delta = \frac{a}{\lambda}$.
Here Re and δ are the Reynolds and the wave number respectively.
Using the assumptions of low Reynolds number and large wavelength approximations and ignoring the terms of inertia, we get equations (3.8)-(3.13) simplified as

$$\frac{\partial p}{\partial z} = \frac{1}{r}\frac{\partial}{\partial r}\Big(r\mu\frac{\partial}{\partial r}\Big)u_p, \quad h_1 \leq r \leq h, \tag{3.14}$$

$$\frac{\partial p}{\partial z} = \frac{1}{r}\frac{\partial}{\partial r}\Big(r\frac{\partial}{\partial r}\Big)u_c, \quad \epsilon \leq r \leq h_1. \tag{3.15}$$

The non-dimensional boundary conditions are described as follows

$$u_p = -1 \quad at \quad r = h, \tag{3.16}$$

$$u_c = -1 \quad at \quad r = \epsilon, \tag{3.17}$$

$$u_p = u_c \quad at \quad r = h_1. \tag{3.18}$$

No-slip condition on the tube wall and velocity continuity at the interface are specified in equations (3.16) to (3.18).

3.3 Solutions

Integrating equations (3.14) and (3.15), under the conditions (3.16) to (3.18), we obtain

$$u_p = -1 - \frac{1}{4\mu}\frac{dp}{dz}\Big[h^2 - r^2 + M\log\Big(\frac{r}{h}\Big)\Big], \tag{3.19}$$

$$u_c = -1 - \frac{1}{4}\frac{dp}{dz}\Big[\epsilon^2 - r^2 + M\log\Big(\frac{r}{\epsilon}\Big)\Big], \tag{3.20}$$

with

$$M = \frac{-h^2 + \mu\epsilon^2 + (1-\mu)h_1^2}{\log(\frac{h_1}{h}) - \mu\log(\frac{h_1}{\epsilon})}.$$

The criteria can be used to obtain solutions in terms of stream functions as $\psi_c = 0$ at $r = 0$ and $\psi_p = \frac{q}{2}$ at $r = h$ (Rao and Usha (1995), Usha and Ramachandra Rao (1997)) in equations (3.19) and (3.20). Applying the criteria, we get
for $h_1 \le r \le h$,

$$\psi_p = \frac{q + h^2 - r^2}{2} + \frac{1}{4\mu}\frac{dp}{dz}\Big[\Big(\frac{h^4 + r^4}{4}\Big) - \frac{r^2h^2}{2} - M\Big\{\frac{h^2}{4} + \frac{r^2}{2}\Big(\log\Big(\frac{r}{h}\Big) - \frac{1}{2}\Big)\Big\}\Big], \tag{3.21}$$

and for $\epsilon \le r \le h_1$,

$$\psi_c = \frac{r^2}{2}\Big[-1 - \frac{1}{4}\frac{dp}{dz}\Big\{\epsilon^2 - \frac{r^2}{2} + M\Big\{\log\Big(\frac{r}{\epsilon}\Big) - \frac{1}{2}\Big\}\Big\}\Big]. \tag{3.22}$$

Thus, we can see that if $\mu \to 1$ in the absence of catheter equations (3.21) and (3.22) reduce to Newtonian fluid and for a single fluid case obtained by (Rao and Usha (1995), Usha and Ramachandra Rao (1997)) respectively.
Now using the condition $\psi_p = \frac{q_c}{2}$ at $r = h_1$ (Rao and Usha (1995), Usha and Ramachandra Rao (1997)) in equation (3.21), we get

$$\frac{q_c + h_1^2}{2} = \frac{q + h^2}{2} + \frac{1}{4\mu}\frac{dp}{dz}\Big[\Big(\frac{h^4 + h_1^4}{4}\Big) - \frac{h_1^2h^2}{2} - M\Big\{\frac{h^2}{4} + \frac{h_1^2}{2}\Big(\log\Big(\frac{h_1}{h}\Big) - \frac{1}{2}\Big)\Big\}\Big], \tag{3.23}$$

which is a fourth-degree equation in h_1, a streamline in the flow field. Also using the condition $\psi_c = \frac{q_c}{2}$ at $r = h_1$ in equation (3.22), we get

$$\frac{q_c + h_1^2}{2} = -\frac{1}{4}\frac{dp}{dz}\Big[\frac{h_1^2\epsilon^2}{2} - \frac{h_1^4}{4} + M\Big\{\frac{h_1^2}{2}\Big(\log\Big(\frac{h_1}{\epsilon}\Big) - \frac{1}{2}\Big)\Big\}\Big]. \tag{3.24}$$

It is to be noted that the right side expressions in (3.23) and (3.24) are equal and will lead to the determination of quantities such as the volume flow rate etc., in terms of h_1 and q_c. Instantaneous volume flow rate is thus obtained from (3.23) and (3.24) as

$$q = -h^2 - \frac{1}{8\mu}\frac{dp}{dz}\Big[\, h^4 + (1-\mu)h_1^4 + 2h_1^2(\mu\epsilon^2 - h^2) + M\Big\{-h^2 + (1-\mu)h_1^2 + 2h_1^2 B\Big\}\Big], \quad (3.25)$$

where $B = \Big(\mu \log(\frac{h_1}{\epsilon}) - \log(\frac{h_1}{h})\Big)$.
Using equation (3.24) we write

$$q_c = -h_1^2 - \frac{1}{8}\frac{dp}{dz}\Big[- h_1^4 + 2h_1^2\epsilon^2 + 2M\Big\{h_1^2\Big(\log\Big(\frac{h_1}{\epsilon}\Big) - 1\Big)\Big\}\Big]. \quad (3.26)$$

Since the expression for flow rate q has been found in (3.25), we write

$$\frac{dp}{dz} = \frac{-8\mu(h^2 + q)}{\eta}, \quad (3.27)$$

where $\eta = h^4 + (1-\mu)h_1^4 + 2h_1^2(\mu\epsilon^2 - h^2) + M\Big\{ - h^2 + (1-\mu)h_1^2 + 2h_1^2 B\Big\}$
Following Brasseur et al. (1987), by taking $h_1 = \alpha$ and $h = 1$, we rewrite $\tilde{\eta}$ as

$$\tilde{\eta} = [1 + (1-\mu)\alpha^4 + 2\alpha^2(\mu\epsilon^2 - 1) + N\{-1 + (1-\mu)\alpha^2 + 2\alpha^2 C\}],$$

where $C = \mu\log(\alpha/\epsilon) - \log(\alpha)$ and $N = \frac{-1+\mu\epsilon^2+(1-\mu)\alpha^2}{\log(\alpha)-\mu\log(\alpha/\epsilon)}$.
The pressure is given by

$$\Delta p = \int_0^z \frac{8\mu(q + h^2)}{\eta} dz.$$

Using the expression for wall surface given in equation (3.1) we find, in view of (3.1),

$$\Delta p = \int_0^z \frac{8\mu}{\eta}(q + 1 - 2\phi e^{k(z+t)}\cos^2(\pi z) + \phi^2 e^{2k(z+t)}\cos^4(\pi z))dz.$$

Symbolising $I_1 = \displaystyle\int_0^z \frac{1}{\eta} dz$ and $I_2 = \displaystyle\int_0^z \frac{e^{k(z+t)}\cos^2(\pi z)}{\eta} dz$ and
$I_3 = \displaystyle\int_0^z \frac{e^{2k(z+t)}\cos^4(\pi z)}{\eta} dz$,
we write the above equation as

$$\Delta p = 8\mu[(q+1)I_1 - 2\phi I_2 + \phi^2 I_3]. \quad (3.28)$$

The time-averaged volume flow rate, $\overline{Q}$, is given by

$$\overline{Q} = (q+1) - 2\phi e^{kz}\Big(\frac{e^k-1}{k}\Big) + \phi^2 e^{2kz}\Big(\frac{e^{2k}-1}{2k}\Big), \tag{3.29}$$

which, for k, reduces to that for uniform wave amplitude.
Therefore, using equations (3.28) and (3.29), we get

$$\Delta p = 8\mu\Big[\Big(\overline{Q} + 2\phi e^{kz}\Big(\frac{e^k-1}{k}\Big) - \phi^2 e^{2kz}\Big(\frac{e^{2k}-1}{2k}\Big)\Big)I_1 - 2\phi I_2 + \phi^2 I_3\Big]. \tag{3.30}$$

The pressure that must be applied to achieve $\overline{Q} = 0$ is given by

$$\Delta p_0 = 8\mu\Big[\Big(2\phi e^{kz}\Big(\frac{e^k-1}{k}\Big) - \phi^2 e^{2kz}\Big(\frac{e^{2k}-1}{2k}\Big)\Big)I_1 - 2\phi I_2 + \phi^2 I_3\Big], \tag{3.31}$$

which also, for $k = 0$, reduces to that for uniform wave amplitude.
From equation (3.30), we deduce $\overline{Q}$ as

$$\overline{Q} = \frac{\Delta p}{8\mu I_1} + 2\phi\frac{I_2}{I_1} - 2\phi e^{kz}\Big(\frac{e^k-1}{k}\Big) + \phi^2 e^{2kz}\Big(\frac{e^{2k}-1}{2k}\Big) - \phi^2\frac{I_3}{I_1}. \tag{3.32}$$

The time-averaged flow rate at zero pressure is given by

$$\overline{Q}_0 = 2\phi\frac{I_2}{I_1} - \phi^2\frac{I_3}{I_1} - 2\phi e^{kz}\Big(\frac{e^k-1}{k}\Big) + \phi^2 e^{2kz}\Big(\frac{e^{2k}-1}{2k}\Big). \tag{3.33}$$

From equations (3.32) and (3.33), we get

$$\Delta p = (\overline{Q} - \overline{Q}_0)8\mu I_1, \tag{3.34}$$

from equations (3.31) and (3.33)

$$\Delta p_0 = -8\mu\overline{Q}_0 I_1, \tag{3.35}$$

and thus from (3.34) and (3.35)

$$\overline{Q} = \overline{Q}_0\Big(1 - \frac{\Delta p}{\Delta p_0}\Big). \tag{3.36}$$

The friction force $F_a(= f_a/\pi\lambda c\mu_p)$ at the tube wall across the axial length is now obtained as

$$F_a = \int_0^z h^2\Big(-\frac{dp}{dz}\Big)dz. \tag{3.37}$$

Therefore,

$$F_a = 8\mu\Big(A_1 + (\overline{Q}-1)A_2 + 2\phi\Big(\frac{e^k-1}{k}\Big)A_3 - \phi^2\Big(\frac{e^{2k}-1}{2k}\Big)A_4\Big), \tag{3.38}$$

where, $A_1 = \int_0^z \frac{h^4}{\eta}dz$, $A_2 = \int_0^z \frac{h^2}{\eta}dz$, $A_3 = \int_0^z \frac{h^2}{\eta}e^{kz}dz$ and $A_4 = \int_0^z \frac{h^2}{\eta}e^{2kz}dz$.
The friction force $F_c(= f_c/\pi\lambda c\mu_c)$ at the catheter wall across the axial length is now derived as

$$F_c = \int_0^z \epsilon^2\Big(-\frac{dp}{dz}\Big)dz. \tag{3.39}$$

Thus,

$$F_c = 8\mu\epsilon^2\Big[(\overline{Q}-1)B_1 + \phi\Big(\frac{e^k-1}{k}\Big)B_2 - \phi^2\Big(\frac{e^{2k}-1}{2k}\Big)B_3 + B_4\Big], \tag{3.40}$$

where $B_1 = \int_0^z \frac{1}{\eta}dz$, $B_2 = \int_0^z \frac{e^{kz}}{\eta}dz$, $B_3 = \int_0^z \frac{e^{2kz}}{\eta}dz$ and $B_4 = \int_0^z \frac{h^2}{\eta}dz$.
It should be noted that the results for a single-phase Newtonian viscous fluid are obtained with $\alpha = 1$ and $\mu = 1$. Using $\alpha = 1$, $\mu = 1$, for the no catheter case, the results of Shapiro et al. (1969) are recovered from the current study.

3.4 Numerical results and discussions

The basis of parametric values is the practical aspect. All the parameters are dimensionless. This gives us the freedom to choose values in certain ranges. For example, α is the ratio of the peripheral layer thickness to the tube radius. ϕ can vary from 0 to $1-\epsilon$ and likewise ϕ_1 can vary from 0 to $\alpha-\epsilon_1$. From the anatomical measurement of Xia et al. (2009), the estimated dimensionless ϕ rose from 0.47 to 0.8043, which yielded $k = 0.134$. $\epsilon = 0.1$ is an ideal assignment.

3.4.1 The interface

The interface layer, unlike the formulation of Medhavi and Singh (2012), is dependent on the viscosity ratio of the peripheral layer. The interface is a streamline which is a solution of the fourth-order algebraic equation given in equation (3.23). This is to be noted that μ implicitly appears in (3.23). The pressure gradient term also involves μ as evident from (3.27) in which η itself involves μ. The solutions for different viscosity ratios are plotted in (Fig. 3.2a). $0 \leq \alpha \leq 1$, where 0 indicates the absence of the peripheral layer while 1 refers to no core layer. $\alpha \leq 0.1$ seems to be practical. However, the peripheral layer thickness is set as $\alpha = 0.4$ with $\phi = 0.49$ for plotting graphs. We choose $\alpha = 0.4$ for the sake of clarity only. ϕ, the dimensionless wave-amplitude, can vary from 0 to 1. From the anatomical measurement of Xia et al. (2009), the estimated dimensionless ϕ rose from 0.47 to 0.8043.
It is observed that the interface deviates significantly if the viscosity ratio is changed from 1, which is equivalent to the case of a single layer or two layers having the same viscosity. For smaller values, the peripheral layer is thicker in the contracted regions and thinner in the relaxed regions for the same catheter (Fig. 3.2a). The thickness of the catheter also plays a prominent role. Just like the viscosity ratio, an increase in the thickness of the catheter results in the thickening of the peripheral layer in the contracted zone of the tube and thinning in the relaxed zone (Fig. 3.2b).

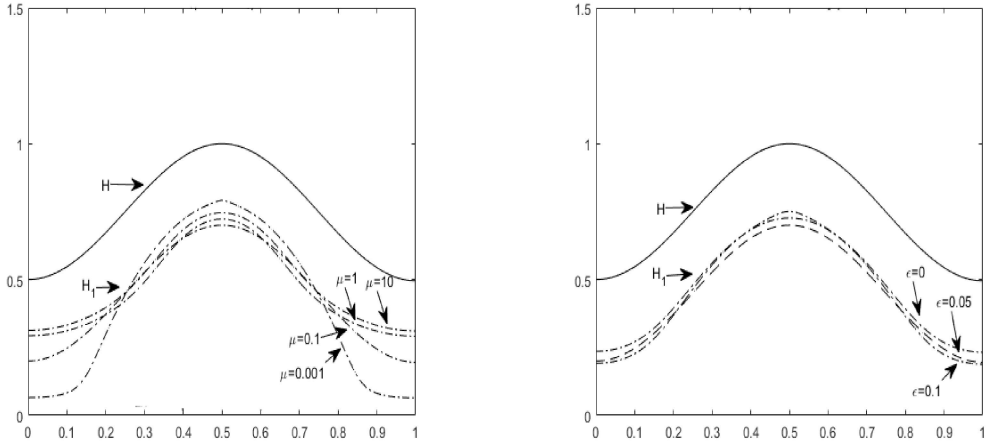

(a) (b)

Figure 3.2: The variation in the shape of the interface for (a) viscosity ratio μ, and (b) catheter size ϵ, $\phi = 0.49$, $\alpha = 0.4$.

3.4.2 Pressure difference vs. flow rate

Equation (3.30) gives a relation between the pressure difference and the time-averaged flow rate. The equations giving the maximum pressure and the maximum time-averaged flow rate are obtained by substituting $\bar{Q} = 0$ in equation (3.30) while the maximum time-averaged flow rate is obtained by replacing Δp by zero in the same equation. The two are given respectively by equations (3.31) and (3.33). The relation is linear, shown in (Fig. 3.3) to (Fig. 3.6), similar to what Brasseur et al. (1987) obtained for flows without the catheter. We observe that even when a catheter is inserted, the flow rate increases with larger wave amplitude (Fig. 3.3). Moreover, the impact of the peripheral layer thickness was tested by varying its thickness in the range of 0.5-1.5. It was observed that the flow rate increases if the peripheral layer thickness α is decreased (Fig. 3.4). Further we examine the flow rate for $\mu = 0.5, 1.0, 1.5$, and find that the flow rate increases with μ (Fig. 3.5). The impact of the dilation parameter was a new dimension to this relation. It is found that the flow rate is immensely affected and increases with the dilation parameter (Fig. 3.6). The physical interpretation is that the flow rate increases if the peripheral layer is

thinner and more viscous. Higher Wave amplitude and larger amplitude dilation increase it further.

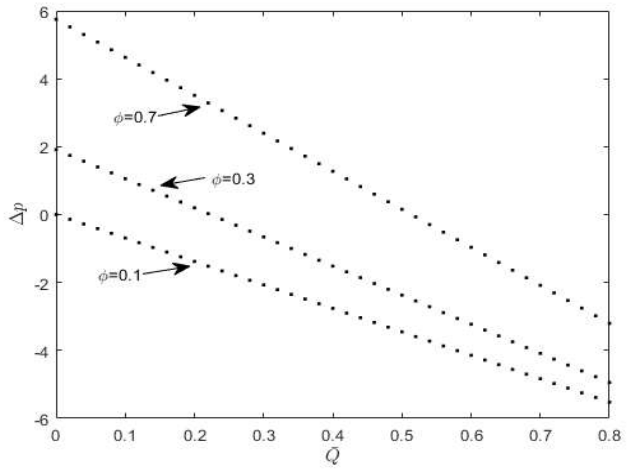

Figure 3.3: Pressure difference Δp vs time-averaged flow rate $\bar{Q}$ for amplitude $\phi = 0.1 - 0.7$, $\alpha = 0.2$, $\mu = 0.3$, $\epsilon = 0.1$.

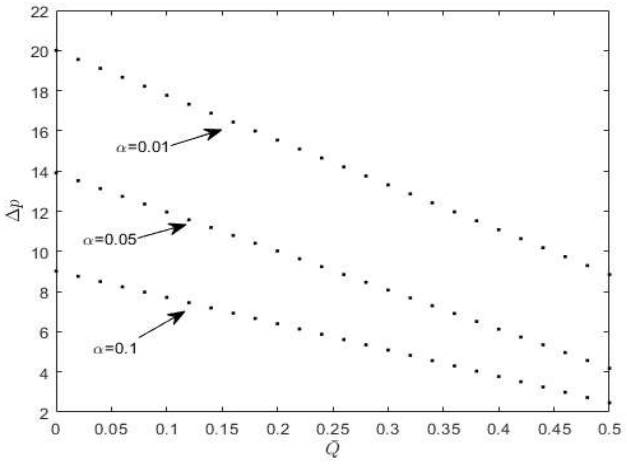

Figure 3.4: Pressure difference Δp vs time-averaged flow rate $\bar{Q}$ for peripheral layer thickness $\alpha = 0.01 - 0.1$, $\phi = 0.49$, $\mu = 1.5$, $\epsilon = 0.1$.

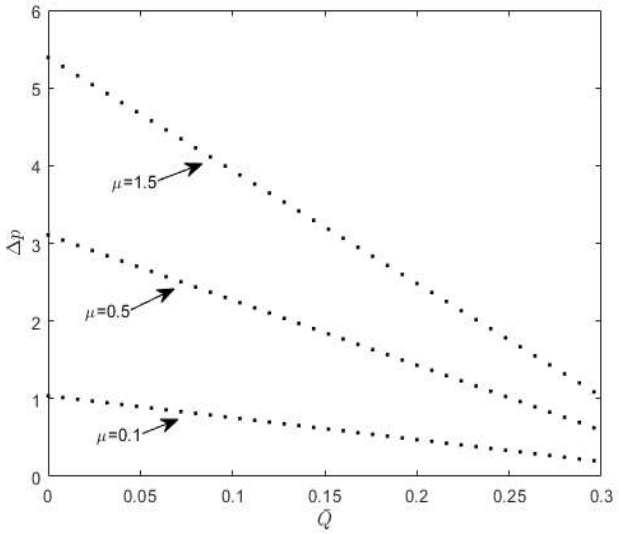

Figure 3.5: Pressure difference Δp vs time-averaged flow rate $\bar{Q}$ for viscosity $\mu = 0.1 - 1.5$ for $\phi = 0.49$, $\alpha = 0.2$, $\epsilon = 0.1$.

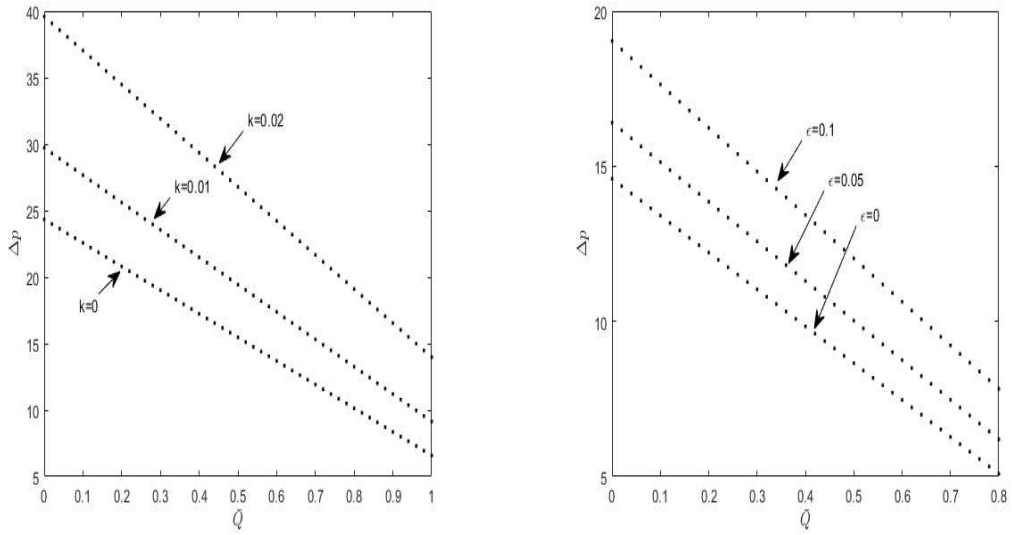

(a) (b)

Figure 3.6: Pressure difference Δp vs time-averaged flow rate $\bar{Q}$ for (a) $k = 0.0 - 0.02$, (b) $\epsilon = 0.0 - 0.1$, $\phi = 0.49$, $\alpha = 0.2$, $\mu = 0.3$.

3.4.3 Pressure distribution

In order to assess the impact of a catheter inserted into oesophagus, we consider a train of four boluses present at a time in the oesophagus. For Newtonian fluids, it is practically possible. We plot the axial pressure distribution with the catheter of radius 0.1 and vary the dilating parameter of the wave amplitude k in the range $0 - 0.02$. This is for the sake of learning the impact, not for quantitative measurement. As per the expectations, the pressure rises progressively (Fig. 3.7). (Fig.3.7) has five parts, viz., (a)-(e) which run from $t = 0.0$ to $t = 1.0$ with an interval of 0.25. Initially, shown in (Fig.3.7), it is observed that pressure rises at the beginning of the tube required for pushing the bolus inside the tube for swallowing. Pressure falls gradually to be negative to facilitate the bolus to move in the tube. However, the pressure rises sharply to create high pressure for pushing the second bolus in the tube. The same rise of pressure restrains the previous bolus so that its motion is controlled. Such a natural mechanism of the flow of a train of boluses protects the oesophagus from frictional forces. Thus, the motion is rhythmic and periodic but controlled. The various pressure curves corresponding to the different values of k indicate how pressure rises with increasing the amplitude dilation parameter. In fact, it is the difference of the pressure from its maximum value to the minimum value that indicates whether pressure increases or decreases. The exclusive description and explanations are available in the research article by Misra and Pandey (2001). The part (b) of the (Fig.3.7) corresponding to $t = 0.25$ shows that the pressure drops to negative values in order to pave the way for a new bolus to enter the tube but at the same time the same pressure rise acting at its head does not allow the bolus ahead of it to come back. Figures 3.7$(c-e)$ simply demonstrate the continuity of the flow with suitable pressure distribution corresponding to all three values of the wave amplitude dilation parameter. This observation is in agreement with the inference drawn during physiological investigations for arteries (Back et al. (1992), Back (1994), Back et al. (1996)). However, it was calculated by Pandey et al. (2017) to be 0.134 for the human oesophagus of length $18cm$ to $25cm$ based on the anatomical measurements of Xia et al. (2009). But this will increase the pressure by many folds. Moreover, keeping $k = 0.01$ constant when we vary ϵ in the range $0 - 0.1$, we observe that pressure rises with the thickness of the catheter (Fig. 3.8). Therefore, the catheter's size needs to be predecided before insertion, depending on

the pressure rise with which the oesophagus is comfortable. Besides, it is concluded that the catheter's insertion should be restricted to an optimum point where it is sufficient for feeding a patient. The reason is that due to reflux or for any other reason, the liquid passed through the catheter may be back in the oesophagus, and secondary peristaltic waves may attempt to push them back to put into the stomach through the cardiac sphincter. Thus, peristaltic action cannot be ruled out even when feeding is done through the catheter.

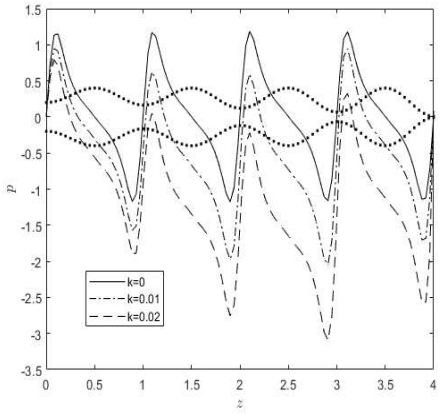

(a)

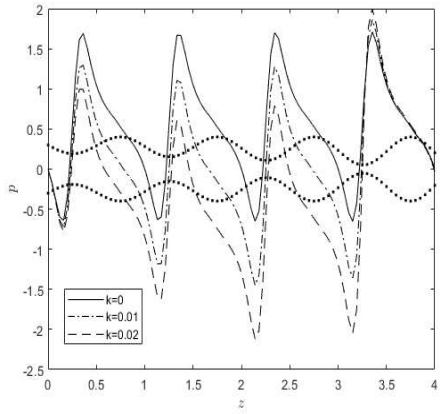

(b)

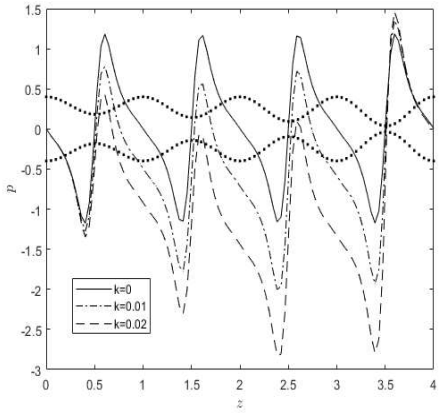

(c)

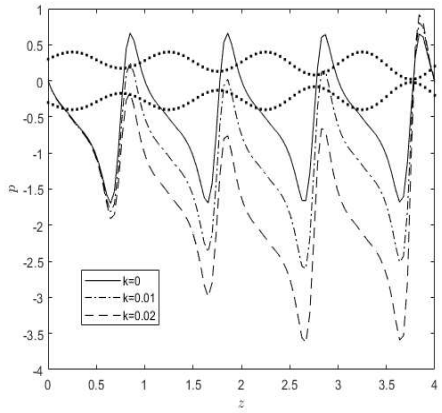

(d)

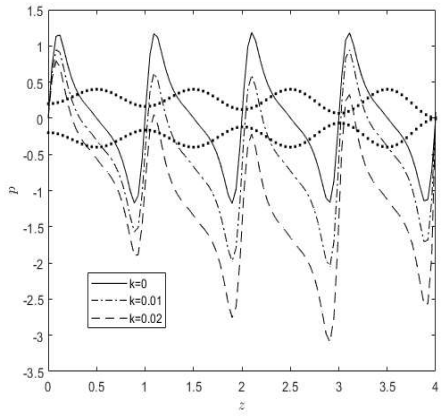

(e)

Figure 3.7: Distribution of pressure p along the axial length z for $k = 0.0-0.02$, $\phi = 0.49$, $\alpha = 0.1$, $\mu = 0.2$, $\epsilon = 0.1$, (a) $t = 0$, (b) $t = 0.25$, (c) $t = 0.5$, (d) $t = 0.75$, (e) $t = 1$.

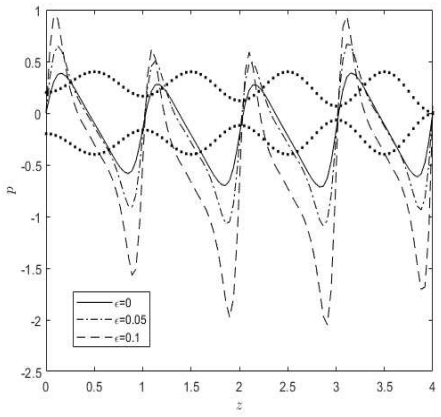

(a)

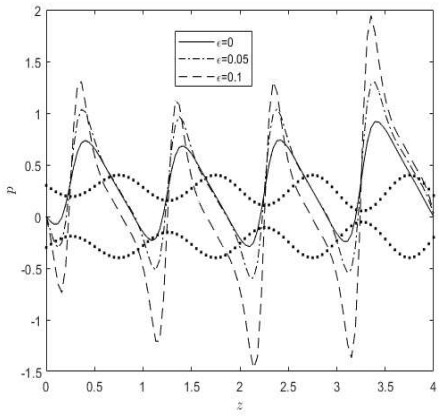

(b)

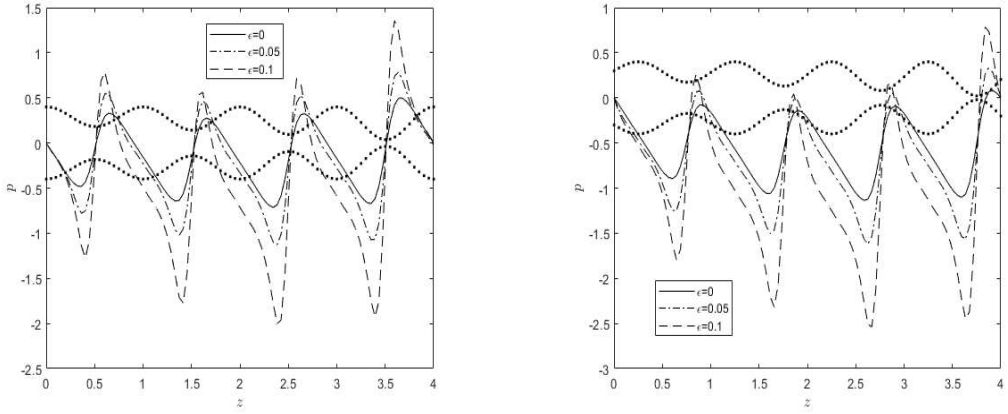

(c)

(d)

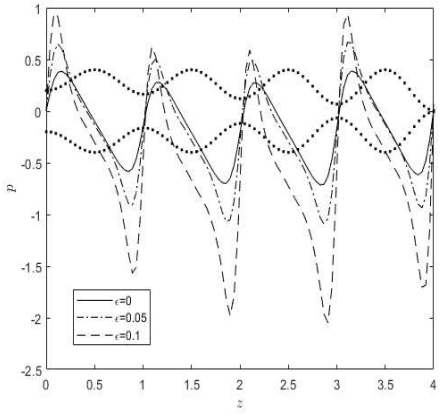

(e)

Figure 3.8: Distribution of pressure p along the axial length z for $\epsilon = 0.0 - 0.1$, $\phi = 0.49$, $\alpha = 0.1$, $\mu = 0.2$, $k = 0.01$ (a) $t = 0$, (b) $t = 0.25$, (c) $t = 0.5$, (d) $t = 0.75$, (e) $t = 1$.

3.4.4 Velocity distribution

The axial velocity profiles are plotted in (Fig. 3.9) for different catheter sizes ϵ varied in the range 0-0.15. It is observed that the axial velocity increases with the catheter thickness for a fixed flow rate all along the axis of the oesophagus. The figures are based on equation (3.19) in which the pressure gradient is given by equation (3.27). This is evident from the fact that pressure increases with the

catheter thickness revealed (Fig 3.8). This can alternatively be interpreted as that in the presence of a catheter if the pressure distribution remains the same, less fluid will flow as the velocity is less. Figs. (3.9) display axial distribution of axial velocity in the Laboratory frame. t is varied in the range 0-1. The wave amplitude dilates progressively. As a consequence, the axial velocity increases as the fluid swallows. The distribution shows that the velocity increases at the tail of the bolus to the maximum and falls to zero at the head of the bolus. It further decreases rapidly to the middle of the contracted region and then once again shoots up to zero at the end of the contracted region. This is the region where the velocity is negative. The next cycle begins after it. It is also observed that the negative velocity in the contracted region increases in magnitude if the catheter is broadened.

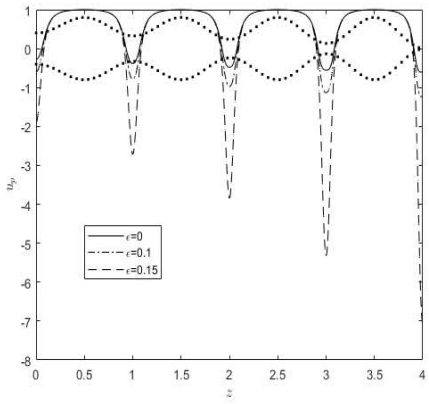

(a)

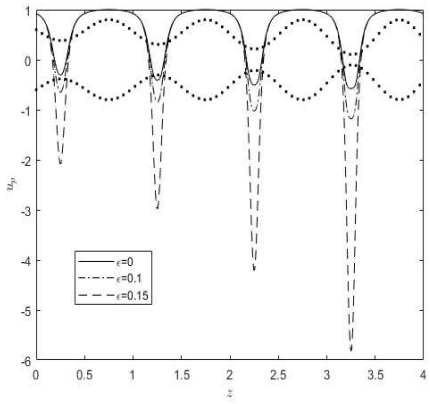

(b)

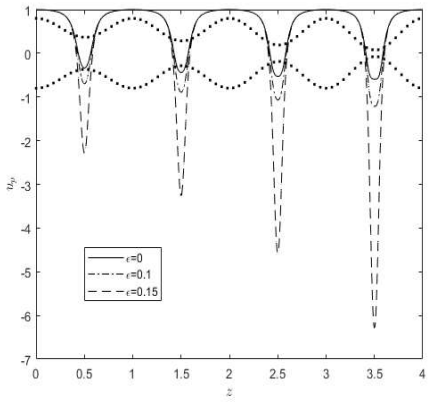

(c)

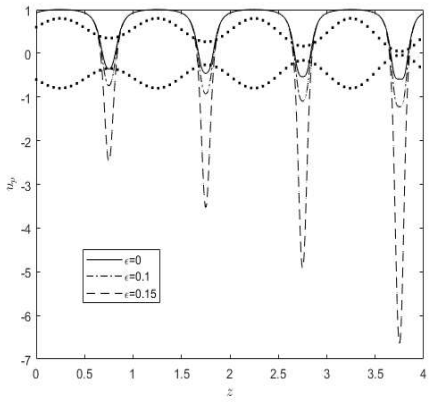

(d)

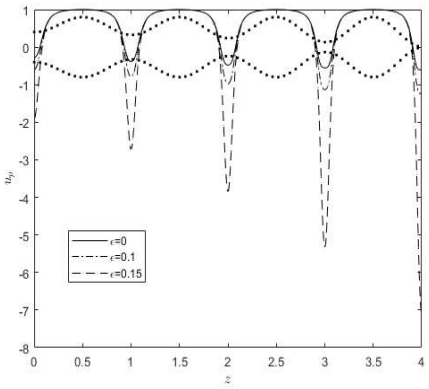

(e)

Figure 3.9: Peripheral layer velocity u_p vs axial length z in the laboratory frame for $\epsilon = 0.0 - 0.1$, $\phi = 0.49$, $\alpha = 0.1$, $\mu = 0.2$, (a) $t = 0$, (b) $t = 0.25$, (c) $t = 0.5$, (d) $t = 0.75$, (e) $t = 1$.

3.4.5 Frictional force

We also plotted the axial distribution of wall frictional forces for the two cases, i.e., with and without a catheter. It is observed that frictional forces are larger when the catheter is introduced in the oesophagus (Fig. 3.10). Frictional resistance requires a decrease in pressure, which is necessary to keep the bolus fluid flowing. As seen in (Fig 3.10), where there are contraction zones close to the tail of the bolus during oesophageal bolus transport, this friction-induced drop in pressure is significant in locations where frictional forces are strong.

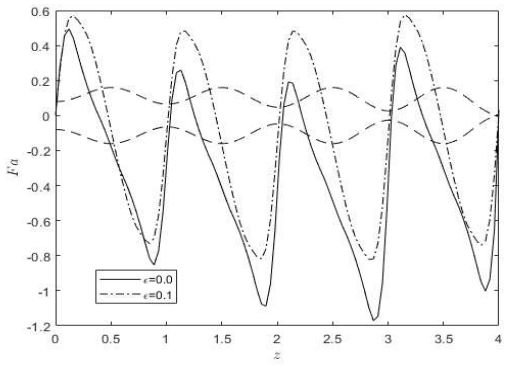

Figure 3.10: Frictional force due to the wall's surface Fa vs the axial length z for ϵ, $\phi = 0.49$, $\alpha = 0.1$, $\mu = 0.2$.

3.5 Conclusions

Non-surgical treatment is used as a first-hand tool to address swallowing disorders. Initially, doctors avoid surgery because post-surgery patients are very likely to suffer from other complications. In the present study, we tried to explore a non-surgical treatment by means of a catheter.

The shape of the interface layer is dependent on the viscosity ratio of the peripheral layer. For smaller values of the viscosity ratio, the peripheral layer is thicker in the contracted regions when the peristaltic waves propagate and thinner in the relaxed regions for the same catheter. An increase in the thickness of the catheter further thickens the peripheral layer in the contracted zone of the tube but results in thinning in the relaxed zone. It is further concluded that the flow rate increases when the peripheral layer is thinner and more viscous. Higher wave amplitude and larger amplitude dilation increase it further.

Pressure obviously rises progressively if the wave amplitude dilates. It also rises with the thickness of the inserted catheter. Therefore, it is concluded that the catheter's insertion should be restricted to an optimal length that is sufficient for feeding a patient. The reason is that due to reflux or for any other reason, the fluid passed through the catheter may be back in the oesophagus, and secondary peristaltic waves may attempt to push them to put into the stomach through the cardiac sphincter. Thus, peristaltic action cannot be ruled out even when feeding is done through the catheter. The increased pressure may cause uneasiness to the patient and sometimes may disturb the feeding process. For similar reasons, no patient should be fed anything directly through the mouth once a catheter has been inserted into the oesophagus through the nose.

Axial velocity also increases with the catheter thickness for a fixed flow rate all along the axis of the oesophagus. This can alternatively be interpreted as that in the presence of a catheter if the pressure distribution remains the same, less fluid will flow as the velocity is less. In the contracted regions, the axial velocity in the laboratory frame is negative. The next cycle begins after it. Further, the negative velocity in the contracted region increases in magnitude if the catheter broadens.

Despite this much exercise, it may be noted that peripheral and core layers have been considered Newtonian. However, the peripheral layer also acts as a lubricant, and the core could be of any type. Hence, non-Newtonian consideration for the two layers will be more appropriate, where Newtonian fluid will be a special case.